Article

An Observer-Based Type-3 Fuzzy Control for Non-Holonomic Wheeled Robots

Hongling Bie [1], Pengyu Li [2,*], Fenghua Chen [3] and Ebrahim Ghaderpour [4,5,*]

[1] Artificial Intelligence Applications College, Shanghai Urban Construction Vocational College, Shanghai 201415, China; biehongling@succ.edu.cn
[2] Shanghai Technician School, Shanghai 200434, China
[3] School of Intelligent Manufacturing, Zhejiang Guangsha Vocational and Technical University of Construction, Dongyang 322100, China; 20192146@zjgsdx.edu.cn
[4] Department of Earth Sciences & CERI Research Centre, Sapienza University of Rome, Piazzale Aldo-Moro, 5, 00185 Rome, Italy
[5] Earth and Space Inc., Calgary, AB T3A 5B1, Canada
* Correspondence: 16221291@simc.cn (P.L.); ebrahim.ghaderpour@uniroma1.it (E.G.)

Abstract: Non-holonomic wheeled robots (NWR) comprise a type of robotic system; they use wheels for movement and offer several advantages over other types. They are efficient, highly, and maneuverable, making them ideal for factory automation, logistics, transportation, and healthcare. The control of this type of robot is complicated, due to the complexity of modeling, asymmetrical non-holonomic constraints, and unknown perturbations in various applications. Therefore, in this study, a novel type-3 (T3) fuzzy logic system (FLS)-based controller is developed for NWRs. T3-FLSs are employed for modeling, and the modeling errors are considered in stability analysis based on the symmetric Lyapunov function. An observer is designed to detect the error, and its effect is eliminated by a developed terminal sliding mode controller (SMC). The designed technique is used to control a case-study NWR, and the results demonstrate the good accuracy of the developed scheme under non-holonomic constraints, unknown dynamics, and nonlinear disturbances.

Keywords: type-3 fuzzy logic; fuzzy control; symmetrical non-holonomic constraints; mobile robots; stability; sliding mode control

1. Introduction

Nowadays, the use of mobile robots in engineering systems is expanding. Therefore, the modeling and control of these systems have attracted the attention of many researchers. Non-holonomic wheeled robots (NWR) are physical systems whose state depends on the path taken to achieve it. Non-holonomic systems cannot be controlled linearly and within the range of each equilibrium point. Therefore, in recent years, several suitable control methods for the stability of these systems have been presented. The performance of the control systems of NWR is greatly reduced under disturbances and restricted constraints and requires further development and study [1,2].

NWRs are only able to move in the direction of the axis of their moving wheels. These limitations make these robots unable to move from one point to another through any path that simply does not have obstacles. On the other hand, the non-linear nature of these systems also makes their control difficult [3]. The sliding-mode controller (SMC) is a robust and effective method for controlling non-linear systems in order to deal with uncertainties and external and internal disturbances and time delays [4]. On the other hand, based on the SMC approach, all modes of the closed-loop system are directed towards a certain sliding surface in space [5]. Rojas-Cubides et al. investigated the control of NWRs in two-dimensional polar coordinates by using the sliding surface tracking control method [6]. In the method presented by Cen and Singh, two controllers for asymptotic stability and tracking error were checked for position and direction, respectively [7].

The methods for controlling NWRs are classified into two general categories: kinematic control and dynamic control. In the last few decades, many studies have been carried out on the kinematic control of NWRs, and less research has been done on the dynamic control of these robots. In engineering applications, dynamic robot controllers are more realistic and valuable than kinematic controllers due to torque input for motors. Therefore, it is better to study the dynamic control of NWRs. It has been shown that non-holonomic systems cannot have a stable and rigid shape with limited movement.

Pai presented a kinematic controller using SMC [8]. The SMC could only ensure the tracking error's convergence toward zero in a constrained manner and therefore could not guarantee the convergence to equilibrium point in a finite amount of time. To solve this problem, the terminal SMC was presented [9]. At first, a model was created to explain the movement dynamics. Following this, an SMC was developed and its control system stability was proven using the Lyapunov theorem. Naderolasli et al. designed a terminal SMC using a high-gain disturbance observer [10]. To account for unmodeled dynamics and unpredictable parameters, an adaptive-neural method was used. The derivative of virtual variables was offered as a solution to the problem of differentiation explosion. Tourajizadeh et al. developed a fast SMC law and suggested a sliding surface disturbance observer to estimate the uncertainty in the system and improve the tracking performance [11]. Disturbance observers make the system robust and improve dynamic performance. Through the use of simulations, the effectiveness of the developed robot in avoiding obstacles as well as the resilience of its related controller in the presence of disturbances are studied. By simulating the system and contrasting the responses of the suggested SMC and feedback linearization approach, these simulations are made valid. Therefore, they are widely used in motion control systems, such as non-holonomic systems and electric charge simulators [12]. Zhai and Song described a path-tracking using SMC and designed an observer [13]. The error was split into a two-order and a three-order subsystem in order to carry out the trajectory tracking task. To stabilize the two-order system in finite time, a fast SMC for angular velocity was first built. Then, the three-order system's stability was ensured by another SMC for linear velocity.

In recent decades, the stabilization of underactive systems has received a lot of attention. The number of control inputs in sub-active systems is less than their degrees of freedoms, and this issue makes their controlling more complicated than in fully active systems. An example of a subactive system is a non-holonomic system. In these systems, internal deformation is considered one of the control factors. On the other hand, based on Brackett's theorem, a smooth and time-independent control law cannot stabilize such systems asymptotically. This theorem has directed researchers' attention to control laws with explicit subordination to time, non-derivative laws, or discontinuous laws. In addition, the geometric perspective has also provided powerful tools for the modeling, analysis, route design, and control and stability of these systems. Therefore, wheeled robots are a group of mobile robots that have movement limitations. These types of robots exhibit highly nonlinear behavior; for this reason, one of the most important topics in the discussion of NWRs is the discussion of path tracking and stability. In [14], the stability of non-holonomic systems was studied in chain form, using the predictive control method [15]. The robust tracking controller based on fuzzy logic for a wheeled kinematic robot with an unknown slip was studied in [16]. Gharajeh and Jond proposed an adaptive controller for reference trajectory tracking by NWRs [17]. Simulations were used to assess the usefulness of the suggested strategy in guiding an NWR through cluttered settings and to show how well it performs in contrast to existing collision-free navigation techniques. The robot's behavior in avoiding obstacles and the length of the path found without colliding were used as the assessment criterion.

To cope with the uncertainties of robotic systems, some FLS-based controllers have been developed. For example, Bi suggested an FLS-based regulator for a wall-cleaning robot to guarantee its operation's safety and dependability [18]. Since the precise underlying dynamics of the vacuum adhesion cannot be analytically represented, an FLS was

employed to accomplish the control goals. Considering symmetry principles in robotic systems, the dynamic modeling by FLSs was studied [18]. Cuevas et al. developed an FLS-based controller for mobile robots using a metaheuristic algorithm [19]. The path-tracking problem of robots using FLSs was studied in [20], and its optimization was investigated by the use of various evolutionary algorithms. Chen et al. developed a type-2 FLS as a controller for class for robotic systems and suggested a genetic algorithm for optimization [21]. The study in [22] proposed a nonlinear FLS-based controller as an analytical design and a straightforward control structure for the trajectory tracking of NWRs. The analytical FLS-based rule was derived by identifying error dynamics. Luviano-Cruz et al. studied the multi-agent robotic systems and suggested an FLS-based Q-function for a reinforcement learning algorithm, which deceased the computational costs and proved the convergence [23]. The symmetrical annular-shaped NWRs were studied in [24], and a modeling scheme was developed.

Recently, T3-FLSs have been introduced by Mohammadzadeh et al. for uncertain complicated systems [25–27]. T3-FLSs are an extension of traditional FLSs that allow for more complex and uncertain reasoning. Unlike type-1 and type-2 FLSs, which use crisp values to represent uncertainty bounds, T3-FLSs use fuzzy sets. This allows for a higher degree of applicability and flexibility in representing uncertainty and reasoning about complex systems. Therefore, the primary advantage of T3-FLSs is their ability to handle more complex and uncertain systems. By allowing for more nuanced reasoning about uncertainty, T3-FLSs can provide more accurate and reliable control of dynamic systems and robots. Additionally, T3-FLSs can be used to model and control systems with multiple inputs and outputs, making them suitable for a wide range of applications.

Another basic advantage of T3-FLSs is their ability to learn fast and adapt over time. By using advanced machine learning techniques to adjust the parameters, T3-FLSs can improve their performance and accuracy over time. This makes them well-suited for applications where the system being controlled may change or evolve over time. Overall, T3-FLSs offer a powerful and flexible tool for modeling and controlling complex and uncertain systems [25,27,28]. However, the application of T3-FLSs in robotic control systems has been rarely investigated. For example, in [26], a T3-FLS was used in control of robotic arms, and the T3-FLS showed a good efficiency and accuracy in the modeling of robotic arms. In [25], a general effective scheme was provided to implement T3-FLS-based controllers for robotic systems and other similar online control problems.

Therefore, in this study we propose a new control strategy on the basis of T3-FLSs. The NWR dynamics are modeled using T3-FLSs with a simple learning strategy, and the estimation error is observed and eliminated by the developed SMC. The main contributions are highlighted as follows:

- A novel approach based on T3-FLSs is introduced to deal with non-holonomic constraints, unknown dynamics, and nonlinear disturbances.
- An observer is designed to detect the error, and its effect is eliminated by a developed terminal sliding mode controller (SMC).
- The modeling errors are considered in stability analysis based on the symmetric Lyapunov function.
- A simple training rule is developed for T3-FLSs.

The remainder of the paper is organized as follows. In Section 2, the dynamics of the case-study system are described. In Section 3, the T3-FLS is illustrated. The controller is designed in Section 4. The simulations and conclusions are provided in Sections 5 and 6, respectively.

2. Problem Formulation

To specify the position of robot, the relationship between the global coordinates and the local coordinates of the robot must be understood. The axis X_I, Y_I is the coordinates in the general reference, indicated by $O : \{X_I, Y_I\}$, as shown in Figure 1. The point P on the robot body is selected in local coordinates to determine the position. Relative to this point, the coordinates $\{X_R, Y_R\}$ are obtained as local coordinates, where the point P is its

origin. The position of a point P in the general coordinates is defined by x and y, and the angle between the axes of general and local coordinates is defined by θ. We represent the position by a vector as:

$$\xi_I = \begin{bmatrix} x \\ y \\ \theta \end{bmatrix} \tag{1}$$

To describe the motion of the robot, we need to convert the motion in global coordinates to the motion along the local axes of the robot. It should be noted that this transformation is a function of the current position. Thus,

$$R(\theta) = \begin{bmatrix} \cos\theta & \sin\theta & 0 \\ -\sin\theta & \cos\theta & 0 \\ 0 & 0 & 1 \end{bmatrix} \tag{2}$$

$R(\theta)$ is used in the motion map in the general reference coordinates $\{X_I, Y_I\}$ and in the local reference frame with coordinates $\{X_R, Y_R\}$.
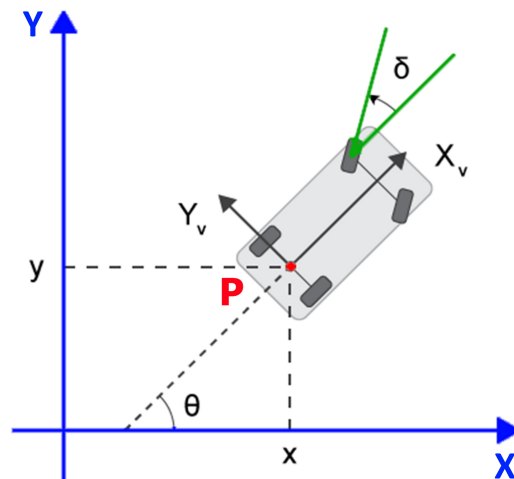

Figure 1. Position of robot.

In the robotics community, the concept of holonomy is used when describing the movement space of moving robots. Such a term can be generalized to many mathematical cases, including differential relations, functions, and limits. An omnidirectional robot that can move in all directions x, y, θ and at any time is holonomic. In mobile robots, this term refers to the kinetic limitation of its chassis [29,30].

In classical mechanics, a system is called holonomic if all the constraints of that system are holonomic. To be a holonomic adverb, it must be functionally expressed as:

$$f(x_1, x_2, \ldots x_n, t) = 0 \tag{3}$$

These restrictions are only dependent on time and coordinates. Constraints that cannot be expressed as a function above are called non-holonomic constraints.

NWRs are nonlinear systems that usually have certain restrictions on their movement. Therefore, the theory of nonlinear control plays a key role in this. Like any system, the goal of controlling wheeled robots is to achieve the desired performance according to the user's taste. Basically, this desirable performance is influenced by the practical conditions of the system. Motion planning and control for wheeled robots are more than two decades old. Apart from the desired control goal for the NWRs, the results in this field can be categorized. Perhaps the most important and major of these categories is based on the coordinates of the mathematical model, for which the design is done [31,32]. The mathematical model of many mechanical systems, including most wheeled robots, is transformed into a standard form by

a transformation from its original coordinates to other coordinates. These transformations are usually in the form of a variable change in states along with feedback in system inputs. In this way, instead of designing the path and control for a specific robotic system, the transformation of the design problem can be solved for the standard form [33,34]. The main advantage of designing for a standard form is that if we can solve the design problem for that form, we have solved the problem at least locally for all systems that can be converted to that form. Another great advantage of this work is that, compared to the original nonlinear system, the standard forms are more prone to having principled methods to solve problems such as point stabilization. In addition, it is usually easier to reach solutions that include a certain type of optimization in the transformed coordinates than in the original coordinates. Of course, solving the problem for standard forms is also difficult. The most obvious difficulty is the unclear relationship between the features of the solution in the transformed coordinates and the features of the solution in the original coordinates. Additionally, it may be very difficult to find a conversion that takes the original system into standard form. Chain systems are a popular standard form that is locally equivalent to many mechanical systems, including wheeled robots [35,36].

Definition 1. *The constraint $A(q)\dot{q} = 0$, where $A(q) \in R^{k \times n}$, and k denotes an independent rate constraint, is called a Faffin restriction. A Fafini constraint is integrable if*

$$A(q)\dot{q} = 0 \Leftrightarrow \frac{\partial h}{\partial q}\dot{q} = 0 \qquad (4)$$

Definition 2. *If a Faffin restriction is integrable, then it is a holonomic restriction; otherwise, it is a non-holonomic restriction.*

Non-holonomic systems cannot be controlled linearly and within the range of their equilibrium point due to the presence of constraints, so we use FLS-based SMC for the stability of this class of systems. Under disturbances, the performance of the control system is greatly reduced. To compensate for the disturbance effect, we use the disturbance observer. The disturbance observer makes the system resistant and improves dynamic performance. The suggested scheme is illustrated in Figure 2.
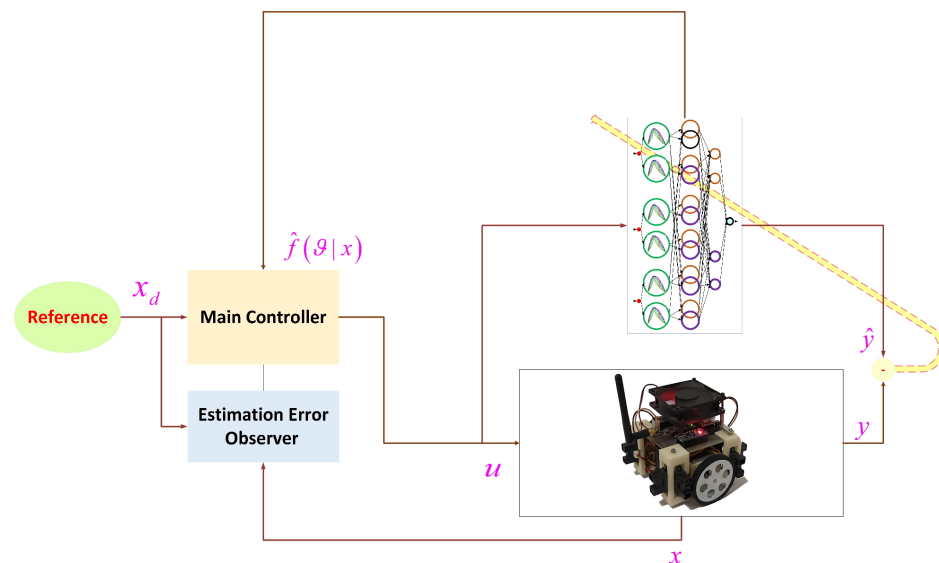

Figure 2. The control diagram.

3. Type-3 Fuzzy Estimator

The nonlinear functions are estimated by T3-FLS, as shown in Figure 3. T3-FLSs show better performance in the face of nonlinear problems [37].
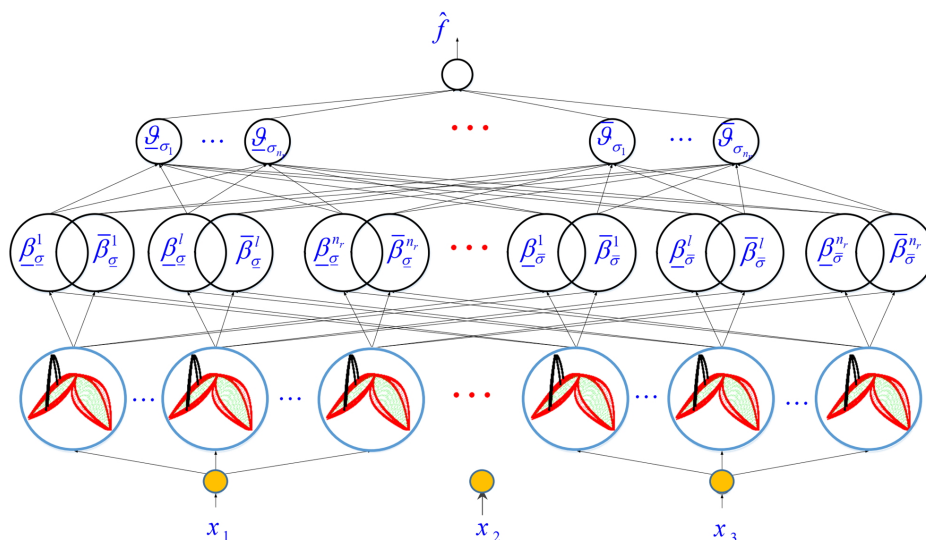
Figure 3. The T3-FLS structure.

In this section, the structure is explained, and rules are optimized.

(1) The inputs are considered as x_1, x_2, x_3.

(2) Compute the memberships. In T3-FLSs, we need to compute the upper/lower memberships for the left and right side of fuzzy sets. Consider $\tilde{\Xi}_i^j$ as jth FS for x_i; then, we have [38] (see Figure 4):

$$
\bar{Z}_{\tilde{\Xi}_i^j \mid \bar{\sigma}_i} = \begin{cases}
1 - \left(\dfrac{\left| x_i - C_{\tilde{\Xi}_i^j} \right|}{\underline{\varsigma}_{\tilde{\Xi}_i^j}} \right)^{\bar{\sigma}_i} & \text{if } C_{\tilde{\Xi}_i^j} - \underline{\varsigma}_{\tilde{\Xi}_i^j} < x_i \leq C_{\tilde{\Xi}_i^j} \\[3ex]
1 - \left(\dfrac{\left| x_i - C_{\tilde{\Xi}_i^j} \right|}{\bar{\varsigma}_{\tilde{\Xi}_i^j}} \right)^{\bar{\sigma}_i} & \text{if } C_{\tilde{\Xi}_i^j} < x_i \leq C_{\tilde{\Xi}_i^j} + \bar{\varsigma}_{\tilde{\Xi}_i^j} \\[3ex]
0 & \text{if } x_i > C_{\tilde{\Xi}_i^j} + \bar{\varsigma}_{\tilde{\Xi}_i^j} \text{ or } x_i \leq C_{\tilde{\Xi}_i^j} - \underline{\varsigma}_{\tilde{\Xi}_i^j}
\end{cases}
\tag{5}
$$

$$
\bar{Z}_{\tilde{\Xi}_i^j \mid \underline{\sigma}_i} = \begin{cases}
1 - \left(\dfrac{\left| x_i - C_{\tilde{\Xi}_i^j} \right|}{\underline{\varsigma}_{\tilde{\Xi}_i^j}} \right)^{\underline{\sigma}_i} & \text{if } C_{\tilde{\Xi}_i^j} - \underline{\varsigma}_{\tilde{\Xi}_i^j} < x_i \leq C_{\tilde{\Xi}_i^j} \\[3ex]
1 - \left(\dfrac{\left| x_i - C_{\tilde{\Xi}_i^j} \right|}{\bar{\varsigma}_{\tilde{\Xi}_i^j}} \right)^{\underline{\sigma}_i} & \text{if } C_{\tilde{\Xi}_i^j} < x_i \leq C_{\tilde{\Xi}_i^j} + \bar{\varsigma}_{\tilde{\Xi}_i^j} \\[3ex]
0 & \text{if } x_i > C_{\tilde{\Xi}_i^j} + \bar{\varsigma}_{\tilde{\Xi}_i^j} \text{ or } x_i \leq C_{\tilde{\Xi}_i^j} - \underline{\varsigma}_{\tilde{\Xi}_i^j}
\end{cases}
\tag{6}
$$

$$
\underline{Z}_{\tilde{\Xi}_i^j \mid \bar{\sigma}_i} = \begin{cases}
1 - \left(\dfrac{\left| x_i - C_{\tilde{\Xi}_i^j} \right|}{\underline{\varsigma}_{\tilde{\Xi}_i^j}} \right)^{\frac{1}{\bar{\sigma}_i}} & \text{if } C_{\tilde{\Xi}_i^j} - \underline{\varsigma}_{\tilde{\Xi}_i^j} < x_i \leq C_{\tilde{\Xi}_i^j} \\[3ex]
1 - \left(\dfrac{\left| x_i - C_{\tilde{\Xi}_i^j} \right|}{\bar{\varsigma}_{\tilde{\Xi}_i^j}} \right)^{\frac{1}{\bar{\sigma}_i}} & \text{if } C_{\tilde{\Xi}_i^j} < x_i \leq C_{\tilde{\Xi}_i^j} + \bar{\varsigma}_{\tilde{\Xi}_i^j} \\[3ex]
0 & \text{if } x_i > C_{\tilde{\Xi}_i^j} + \bar{\varsigma}_{\tilde{\Xi}_i^j} \text{ or } x_i \leq C_{\tilde{\Xi}_i^j} - \underline{\varsigma}_{\tilde{\Xi}_i^j}
\end{cases}
\tag{7}
$$

$$
\underline{Z}_{\tilde{\Xi}_i^j \,|_{\underline{\varrho}_i}} =
\begin{cases}
1 - \left(\dfrac{\left| x_i - C_{\tilde{\Xi}_i^j} \right|}{\varsigma_{\underline{\tilde{\Xi}}_i^j}} \right)^{\frac{1}{\underline{\varrho}_i}} & \text{if } C_{\tilde{\Xi}_i^j} - \underline{\varsigma}_{\underline{\tilde{\Xi}}_i^j} < x_i \le C_{\tilde{\Xi}_i^j} \\[3ex]
1 - \left(\dfrac{\left| x_i - C_{\tilde{\Xi}_i^j} \right|}{\bar{\varsigma}_{\underline{\tilde{\Xi}}_i^j}} \right)^{\frac{1}{\underline{\varrho}_i}} & \text{if } C_{\tilde{\Xi}_i^j} < x_i \le C_{\tilde{\Xi}_i^j} + \bar{\varsigma}_{\underline{\tilde{\Xi}}_i^j} \\[3ex]
0 & \text{if } x_i > C_{\tilde{\Xi}_i^j} + \bar{\varsigma}_{\tilde{\Xi}_i^j} \text{ or } r\, x_i \le C_{\tilde{\Xi}_i^j} - \underline{\varsigma}_{\tilde{\Xi}_i^j}
\end{cases}
\tag{8}
$$

where $\bar{Z}_{\tilde{\Xi}_i^j \,|_{\bar{\sigma}_i}} / \bar{Z}_{\tilde{\Xi}_i^j \,|_{\underline{\varrho}_i}}$, and $\underline{Z}_{\tilde{\Xi}_i^j \,|_{\bar{\sigma}_i}} / \underline{Z}_{\tilde{\Xi}_i^j \,|_{\underline{\varrho}_i}}$ denote the upper/lower. Additionally, $C_{\tilde{\Xi}_i^j}$ represents the center of $\tilde{\Xi}_i^j$, and $\underline{\varsigma}_{\tilde{\Xi}_i^j}$ and $\bar{\varsigma}_{\tilde{\Xi}_i^j}$ show the distances between $C_{\tilde{\Xi}_i^j}$ and the left/right points of $\tilde{\Xi}_i^j$ (see Figure 4).
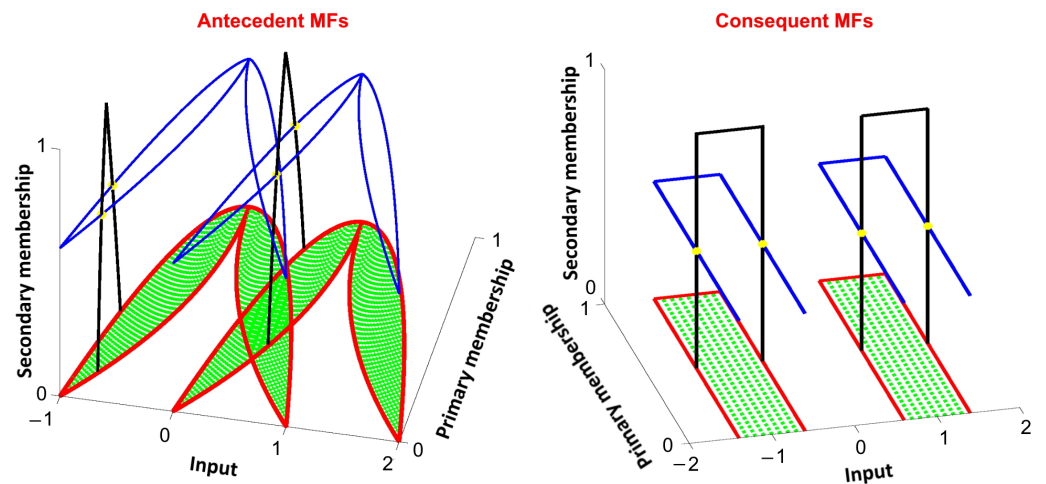

Figure 4. Type-3 fuzzy set.

(3) By considering the upper/lower memberships, the corresponding firing degree of rules are written as:

$$
\bar{\beta}_{\bar{\sigma}_i}^l = \bar{Z}_{\tilde{\Xi}_1^{p_1} \,|_{\bar{\sigma}_i}} \cdot \bar{Z}_{\tilde{\Xi}_1^{p_2} \,|_{\bar{\sigma}_i}} \cdots \bar{Z}_{\tilde{\Xi}_1^{p_n} \,|_{\bar{\sigma}_i}}
\tag{9}
$$

$$
\bar{\beta}_{\underline{\varrho}_i}^l = \bar{Z}_{\tilde{\Xi}_1^{p_1} \,|_{\underline{\varrho}_i}} \cdot \bar{Z}_{\tilde{\Xi}_1^{p_2} \,|_{\underline{\varrho}_i}} \cdots \bar{Z}_{\tilde{\Xi}_1^{p_n} \,|_{\underline{\varrho}_i}}
\tag{10}
$$

$$
\underline{\beta}_{\bar{\sigma}_i}^l = \underline{Z}_{\tilde{\Xi}_1^{p_1} \,|_{\bar{\sigma}_i}} \cdot \underline{Z}_{\tilde{\Xi}_1^{p_2} \,|_{\bar{\sigma}_i}} \cdots \underline{Z}_{\tilde{\Xi}_1^{p_n} \,|_{\bar{\sigma}_i}}
\tag{11}
$$

$$
\underline{\beta}_{\underline{\varrho}_i}^l = \underline{Z}_{\tilde{\Xi}_1^{p_1} \,|_{\underline{\varrho}_i}} \cdot \underline{Z}_{\tilde{\Xi}_1^{p_2} \,|_{\underline{\varrho}_i}} \cdots \underline{Z}_{\tilde{\Xi}_1^{p_n} \,|_{\underline{\varrho}_i}}
\tag{12}
$$

where form of l-th rule is given as:

$$
\begin{aligned}
&\text{If } x_1 \text{ is } \tilde{\Xi}_1^{p_1} \text{ and } x_2 \text{ is } \tilde{\Xi}_2^{p_2} \text{ and } \cdots \quad x_n \text{ is } \tilde{\Xi}_n^{p_n} \\
&\text{Then } f \in \left[\underline{\vartheta}_l, \bar{\vartheta}_l \right], l = 1, \dots, M
\end{aligned}
\tag{13}
$$

where $\underline{\vartheta}_l \in \left[\underline{\vartheta}_{l,\underline{\varrho}}, \underline{\vartheta}_{l,\bar{\sigma}} \right]$, $\bar{\vartheta}_l \in \left[\bar{\vartheta}_{l,\underline{\varrho}}, \bar{\vartheta}_{l,\bar{\sigma}} \right]$, $\tilde{\Xi}_i^{p_j}$ denotes the FS for x_i, and $\underline{\vartheta}_l$ and $\bar{\vartheta}_l$ represent the rule parameters.

(4) Considering the simple type-reduction, the output is given as:

$$f = \frac{\sum\limits_{i=1}^{n_\sigma} \left(\underline{\sigma}_i \underline{\ell}_i + \bar{\sigma}_i \bar{\ell}_i \right)}{\sum\limits_{i=1}^{n_\sigma} \left(\underline{\sigma}_i + \bar{\sigma}_i \right)} \tag{14}$$

where

$$\bar{\ell}_i = \frac{\sum\limits_{l=1}^{n_r} \left(\bar{\beta}_{\bar{\sigma}_i}^l \bar{\vartheta}_{l,\bar{\sigma}_i} + \underline{\beta}_{\bar{\sigma}_i}^l \underline{\vartheta}_{l,\bar{\sigma}_i} \right)}{\sum\limits_{l=1}^{n_r} \left(\bar{\beta}_{\bar{\sigma}_i}^l + \underline{\beta}_{\bar{\sigma}_i}^l \right)} \tag{15}$$

$$\underline{\ell}_i = \frac{\sum\limits_{l=1}^{n_r} \left(\bar{\beta}_{\underline{\sigma}_i}^l \bar{\vartheta}_{l,\underline{\sigma}_i} + \underline{\beta}_{\underline{\sigma}_i}^l \underline{\vartheta}_{l,\underline{\sigma}_i} \right)}{\sum\limits_{l=1}^{n_r} \left(\bar{\beta}_{\underline{\sigma}_i}^l + \underline{\beta}_{\underline{\sigma}_i}^l \right)} \tag{16}$$

The output $f(X, \vartheta)$ is rewritten as:

$$f(X, \vartheta) = \vartheta^T \Omega \tag{17}$$

where

$$\Omega^T = \left[\underline{\Omega}_{1,\underline{\sigma}_i}, \ldots, \underline{\Omega}_{n_r,\underline{\sigma}_i}, \underline{\Omega}_{1,\bar{\sigma}_i}, \ldots, \underline{\Omega}_{n_r,\bar{\sigma}_i}, \bar{\Omega}_{1,\underline{\sigma}_i}, \ldots, \bar{\Omega}_{n_r,\underline{\sigma}_i}, \bar{\Omega}_{1,\bar{\sigma}_i}, \ldots, \bar{\Omega}_{n_r,\bar{\sigma}_i} \right] \tag{18}$$

$$\vartheta^T = \left[\underline{\vartheta}_{1,\underline{\sigma}_i}, \ldots, \underline{\vartheta}_{n_r,\underline{\sigma}_i}, \underline{\vartheta}_{1,\bar{\sigma}_i}, \ldots, \underline{\vartheta}_{n_r,\bar{\sigma}_i}, \bar{\vartheta}_{1,\underline{\sigma}_i}, \ldots, \bar{\vartheta}_{n_r,\underline{\sigma}_i}, \bar{\vartheta}_{1,\bar{\sigma}_i}, \ldots, \bar{\vartheta}_{n_r,\bar{\sigma}_i} \right] \tag{19}$$

$$\underline{\Omega}_{l,\underline{\sigma}_i} = \frac{\sum\limits_{i=1}^{n_\sigma} \underline{\sigma}_i \underline{\beta}_{\underline{\sigma}_i}^l}{\sum\limits_{i=1}^{n_\sigma} \left(\underline{\sigma}_i + \bar{\sigma}_i \right) \sum\limits_{l=1}^{n_r} \left(\bar{\beta}_{\underline{\sigma}_i}^l + \underline{\beta}_{\underline{\sigma}_i}^l \right)} \tag{20}$$

$$\bar{\Omega}_{l,\underline{\sigma}_i} = \frac{\sum\limits_{i=1}^{n_\sigma} \underline{\sigma}_i \bar{\beta}_{\underline{\sigma}_i}^l}{\sum\limits_{i=1}^{n_\sigma} \left(\underline{\sigma}_i + \bar{\sigma}_i \right) \sum\limits_{l=1}^{n_r} \left(\bar{\beta}_{\underline{\sigma}_i}^l + \underline{\beta}_{\underline{\sigma}_i}^l \right)} \tag{21}$$

$$\underline{\Omega}_{l,\bar{\sigma}} = \frac{\sum\limits_{i=1}^{n_\sigma} \bar{\sigma}_i \underline{\beta}_{\bar{\sigma}}^l}{\sum\limits_{i=1}^{n_\sigma} \left(\underline{\sigma}_i + \bar{\sigma}_i \right) \sum\limits_{l=1}^{n_r} \left(\bar{\beta}_{\bar{\sigma}}^l + \underline{\beta}_{\bar{\sigma}}^l \right)} \tag{22}$$

$$\bar{\Omega}_{l,\bar{\sigma}} = \frac{\sum\limits_{i=1}^{n_\sigma} \bar{\sigma}_i \bar{\beta}_{\bar{\sigma}}^l}{\sum\limits_{i=1}^{n_\sigma} \left(\underline{\sigma}_i + \bar{\sigma}_i \right) \sum\limits_{l=1}^{n_r} \left(\bar{\beta}_{\bar{\sigma}}^l + \underline{\beta}_{\bar{\sigma}}^l \right)} \tag{23}$$

The rules are updated as:

$$\vartheta(t) = \vartheta(t-1) + \varepsilon \Omega (y - \hat{y}) \tag{24}$$

4. Controller

We describe the third-order non-holonomic system in chain form as follows:

$$\begin{aligned}
\dot{x}_1 &= u_1 \\
\dot{x}_2 &= u_2 \\
\dot{x}_3 &= f(x) + x_2 u_1 + n
\end{aligned} \tag{25}$$

where $x = [x_1, x_2, x_3]^T$, and u_1 and u_2 are controllers. $\hat{f}(\vartheta, x)$ is a nonlinear function, and n denotes the disturbance. The dynamics of robot are written as:

$$\begin{aligned}
\dot{x}_1 &= u_1 \\
\dot{x}_2 &= u_2 \\
\dot{x}_3 &= \hat{f}(\vartheta|x) + x_2 u_1 + \varphi
\end{aligned} \tag{26}$$

where $\hat{f}(\vartheta|x)$ denotes the T3-FLS and φ represents the estimation error. If the desired path is $x_\varphi = [x_{1d}, x_{2d}, x_{3\varphi}]^T$, then we can write:

$$\begin{aligned}
\dot{x}_{1d} &= u_{1d} \\
\dot{x}_{2d} &= u_{2d} \\
\dot{x}_{3\varphi} &= f(x_\varphi) + x_{2d} u_{1d}
\end{aligned} \tag{27}$$

where u_{1d} and u_{2d} are the desired controllers. Consider the tracking error as $x_e = x - x_\varphi$, then we can write:

$$\begin{aligned}
\dot{x}_{1e} &= u_1 - u_{1d} \\
\dot{x}_{2e} &= u_2 - u_{2d} \\
\dot{x}_{3e} &= (-u_{1d} + u_1)(x_{2d} + x_{2e}) + u_{1d} x_{2e} + f(x) - f(x_\varphi) + \varphi
\end{aligned} \tag{28}$$

Rewrite the system dynamics as:

$$\dot{u}_1 = v_1 \dot{u}_2 = v_2 \tag{29}$$

From (28) and (29), we can write:

$$\begin{aligned}
\dot{x}_{1e} &= u_1 - u_{1d} \\
\dot{u}_1 &= v_1
\end{aligned} \tag{30}$$

The controller v_1 is considered as follows:

$$v_1 = \dot{u}_{1d} - 2 x_{1e}^{-0.4}(-u_{1d} + u_1) - 4(5 x_{1e}^{0.6} - u_{1d} + u_1)^{0.6} \tag{31}$$

This controller guarantee that $-u_{1d} + u_1$ and x_{1e} are approached to zero. From (28) and (29), consider the second subsystem:

$$\begin{aligned}
\dot{x}_{2e} &= u_2 - u_{2d} \\
\dot{x}_{3e} &= x_{2e} u_{1d} + f(x) - f(x_\varphi) + \varphi \\
\dot{u}_2 &= v_2
\end{aligned} \tag{32}$$

The sliding surface s as:

$$s = \eta - x_3 \tag{33}$$

$\dot{\eta}$ is written as:

$$\dot{\eta} = -ks - \mu \tanh(s) - \varepsilon s^{a_0/b_0} - |f(x)| \tanh(s) + x_2 u_1 \tag{34}$$

The parameters a_0 and b_0 are positive constant, and $a_0 < b_0$. The other parameters k, μ, and ε are also positive constant, and $\mu \geq |\varphi|$. The disturbance estimation error $\hat{\varphi}$ is written as:

$$\hat{\varphi} = -ks - \varepsilon s^{a_0/b_0} - \mu \tanh(s) - f(x) - |f(x)| \tanh(s) \tag{35}$$

In the following, it is proved that $\hat{\varphi}$ approaches zero. By taking derivative from (33), we can write:

$$\dot{s} = \dot{\eta} - \dot{x}_3 = -ks - \mu \tanh(s) - \varepsilon s^{a_0/b_0} - |f(x)| \tanh(s) - f(x) - \varphi \tag{36}$$

Consider the Lyapunov function $V(s)$ as:

$$V(s) = \frac{1}{2}s^2 \tag{37}$$

Derivative of (37), and substituting from (36) yields:

$$
\begin{aligned}
\dot{V}(s) &= s\dot{s} \\
&= s\left(-ks - \varepsilon s^{a_0/b_0} - \mu \tanh(s) - f(x) - |f(x)|\tanh(s) - \varphi\right) \\
&\leq -ks^2 - \varepsilon s^{(a_0+b_0)/b_0} - \mu|s| - sf(x) + |s||\varphi| - |f(x)||s| \\
&\leq -ks^2 - \varepsilon s^{(a_0+b_0)/b_0} \\
&\leq -2kV(s) - 2^{(a_0+b_0)/2b_0}\varepsilon V(s)^{(a_0+b_0)/2b_0}
\end{aligned}
\tag{38}
$$
$$\tag{39}$$

Then, it is concluded from the terminal SMC theorem that s is converged to zero. The estimation error $\tilde{\varphi}$ is written as:

$$
\begin{aligned}
\tilde{\varphi} &= \hat{\varphi} - \varphi \\
&= -ks - \mu\tanh(s) - \varepsilon s^{a_0/b_0} - |f(x)|\tanh(s) - f(x) - \varphi \\
&= -ks - \mu\tanh(s) - \varepsilon s^{a_0/b_0} - |f(x)|\tanh(s) - f(x) - \dot{x}_3 + f(x) + x_2 u \\
&= -ks - \mu\tanh(s) - \varepsilon s^{a_0/b_0} - |f(x)|\tanh(s) - \dot{x}_3 + x_2 u \\
&= \dot{\eta} - \dot{x}_3 = \dot{s}
\end{aligned}
\tag{40}
$$

Considering the convergence of s, the convergence of $\tilde{\varphi}$ is proved. To design the controller, the recursive surface is designed as:

$$
\begin{aligned}
\psi_1 &= x_{2e} + x_{3e} \\
\psi_2 &= \dot{\psi}_1 + \rho_1 \psi_1^{a_1/b_1} \\
\psi_3 &= \dot{\psi}_2 + \rho_2 \psi_2^{a_2/b_2} + s
\end{aligned}
\tag{41}
$$

where ρ_1 and ρ_2 are positive and a_1, a_2, b_1, b_2 are positive integers. For ψ_2 and ψ_3, we can write:

$$
\begin{aligned}
\dot{\psi}_2 &= \ddot{\psi}_1 + \rho_1 \frac{\varphi}{dt}\left(\psi_1^{a_1/b_1}\right) \\
\dot{\psi}_3 &= \ddot{\psi}_2 + \rho_2 \frac{\varphi}{dt}\left(\psi_2^{a_2/b_2}\right) + \dot{s}
\end{aligned}
\tag{42}
$$

The jth-order derivative of ψ_2 and ψ_3 are written as:

$$
\begin{aligned}
\psi_2^{(j)} &= \psi_1^{(j+1)} + \rho_1 \frac{\varphi^{(j)}}{\varphi t^{(j)}}\left(\psi_1^{a_1/b_1}\right) \\
\psi_3^{(j)} &= \psi_2^{(j+1)} + \rho_2 \frac{\varphi^{(j)}}{\varphi t^{(j)}}\left(\psi_2^{a_2/b_2}\right) + s^{(j)}
\end{aligned}
\tag{43}
$$

Then, from Equations (28), (29), and (41) we can write:

$$\psi_1^{(3)} = \dot{v}_2 - \ddot{u}_{2d} + \ddot{x}_{2e}u_{1d} + 2\dot{x}_{2e}\dot{u}_{1d} + x_{2e}\ddot{u}_{1d} + \dot{f}(x) - \dot{f}(x_\varphi) + \ddot{\varphi} \tag{44}$$

From (41), Equation (44) can be written as:

$$
\begin{aligned}
\dot{\psi}_3 &= \psi_1^{(3)} + \sum_{j=1}^{2} \rho_j \frac{\varphi^{(3-j)}}{\varphi t^{(3-j)}} \left(\psi_j^{a_j/b_j} \right) + \dot{s} \\
&= \dot{v}_2 - \ddot{u}_{2d} + \ddot{x}_{2e} u_{1d} + 2\dot{x}_{2e} \dot{u}_{1d} + x_{2e} \ddot{u}_{1d} \\
&\quad + \ddot{f}(x) - \ddot{f}(x_\varphi) + \dddot{\varphi} + \sum_{j=1}^{2} \rho_j \frac{\varphi^{(3-j)}}{\varphi t^{(3-j)}} \left(\psi_j^{a_j/b_j} \right) + \dot{s}
\end{aligned}
\tag{45}
$$

The controller is given as:

$$
\begin{aligned}
\dot{v}_2 &= \ddot{u}_{2d} - \ddot{x}_{2e} u_{1d} - 2\dot{x}_{2e} \dot{u}_{1d} - x_{2e} \ddot{u}_{1d} \\
&\quad - \ddot{f}(x) + \ddot{f}(x_\varphi) + s^{(3)} - \dddot{\varphi} \\
&\quad - \sum_{j=1}^{2} \rho_j \frac{\varphi^{(3-j)}}{\varphi t^{(3-j)}} \left(\psi_j^{a_j/b_j} \right) - \dot{s} - \delta \psi_3 - \zeta \psi_3^{a_3/b_3}
\end{aligned}
\tag{46}
$$

where $\delta > 0$ and $\zeta > 0$. By the controller (46), ψ_1, ψ_2, and ψ_3 are converged to zero. To prove this, from substituting (46) into (45), we write:

$$
\dot{\psi}_3 = -\delta \, \psi_3 - \zeta \, \psi_3^{a_3/b_3}
\tag{47}
$$

Now, consider the following Lyapunov:

$$
V(\psi_i) = \frac{1}{2} \psi_i^T \psi_i
\tag{48}
$$

det $V(\psi_3)$ becomes:

$$
\begin{aligned}
\dot{V}(\psi_3) &= \psi_3^T \dot{\psi}_3 \\
&= -\psi_3^T \left(\delta \, \psi_3 + \zeta \, \psi_3^{a_3/b_3} \right) \\
&\leq -2\delta V(\psi_3) - 2^{\eta_3} \zeta V(\psi_3)^{\eta_3}
\end{aligned}
\tag{49}
$$

where $\eta_3 = \frac{a_3 + b_3}{2b_3}$. Then, $\psi_3 = 0$ is converged to zero. From (41), we can write:

$$
\dot{\psi}_2 = -\rho_2 \psi_2^{a_2/b_2} - s
\tag{50}
$$

Similarly from the theorem of terminal SMC, we can conclude that ψ_2 also reached zero. Then, from (41), we can obtain:

$$
\dot{\psi}_1 = -\rho_1 \psi_1^{a_1/b_1}
\tag{51}
$$

Then, by taking derivative from (51) along with the path ψ_1 and ψ_2, we have:

$$
\begin{aligned}
\dot{V}_1 &= \psi_1^T \dot{\psi}_1 \leq -\rho_1 ||\psi_1||^{\frac{a_1}{b_1}+1} \\
\dot{V}_2 &= \psi_2^T \dot{\psi}_2 \leq -\rho_2 ||\psi_2||^{\frac{a_2}{b_2}+1}
\end{aligned}
\tag{52}
$$

Therefore, it is concluded that all surfaces are converged to zero.

5. Simulation

In this section, the results of simulations are provided. The dynamic of case study robot is written as:

$$\dot{x}_1 = u_1$$
$$\dot{x}_2 = u_2$$
$$\dot{x}_3 = -x_1 + 3x_2(1 - x_1^2) + u_1 x_2 + \cos(0.2\pi t) + 2\cos(0.4\sqrt{t+1}) \qquad (53)$$

where $f = -x_1 + 3x_2(1 - x_1^2) + u_1 x_2$ and $\varphi = \cos(0.2\pi t) + 2\cos(0.4\sqrt{t+1})$. The reference trajectory is considered as:

$$\dot{x}_{1d} = u_{1d}$$
$$\dot{x}_{2d} = u_{2d}$$
$$\dot{x}_{3\varphi} = f(x_\varphi) + x_{2d} u_{1\varphi} \qquad (54)$$

where $f(x_\varphi) = -x_{1d} + 3x_{2d}(1 - x_{1d}^2)$. The dynamics of $x_{ie} = x_i - x_{id}$ $(i = 1, 2, 3)$ are written as:

$$\dot{x}_{1e} = u_1 - u_{1d}$$
$$\dot{x}_{2e} = u_2 - u_{2d}$$
$$\dot{x}_{3e} = (-u_{1d} + u_1)x_2 + x_{2e} u_{1d} + \varphi - f(x_\varphi) + f(x) \qquad (55)$$

The parameters considered are given in Table 1. As mentioned earlier, the controller accuracy does not depend on the system dynamics and parameters. However, there are some free parameters in the suggested control system that have light restrictions on their values. The values of these parameters are given in Table 1.

Table 1. Control conditions.

Parameter	Value
k	10
b_2	7
b_1	9
a_1	5
b_0	5
a_0	3
ε	3
μ	2
δ	5
ρ_2	2
ρ_1	3
ζ	1.5

The initialization is considered as $u_1(0) = 3$, $u_2(0) = -2$ and $\eta(0) = 0.6$. The inputs for reference system are:

$$u_{2d} = 1 - e^{-4t}$$
$$u_{1d} = 1 - e^{-2t} \qquad (56)$$

The performances are illustrated in Figure 5. The tracking errors for x_1, x_2, and x_3 are also illustrated in Figure 6, showing that the error approaches zero in a short time. The errors do not have sudden spikes or drops, indicating good stability in the tracking system. The errors steadily decrease until they reach an acceptable level of accuracy. The trajectories also show that the tracking system is able to quickly adapt to changes in the environment, such as perturbation by external disturbances. This means the tracking errors quickly adjust to maintain accuracy in the presence of uncertainties and perturbations.

The key to a successful implementation of SMC is the design of good control signals that can drive the system's state onto the sliding surface and maintain stability on the

surface. The sliding surface is a virtual boundary that separates the system's behavior into two distinct regions: one where the system's behavior is stable, and the other where the system's behavior is unstable. The goal of SMC is to keep the system's behavior on the stable region of the sliding surface. The signals of controllers, shown in Figure 7, demonstrate a rapid convergence to the sliding surface, stability on the surface, and robustness to disturbances and uncertainties. The trajectory of the control signal reflects these goals, with rapid adjustments to drive the system onto the surface and small adjustments to maintain stability once on the surface. These signals also show the small overshoots and oscillations during the transition to the sliding surface.

The sliding surfaces are shown in Figure 8. The trajectory of the sliding surfaces shows a rapid convergence to the desired surface, with minimal oscillations or overshoot. Once on the sliding surface, the trajectory remains relatively flat and stable, with small adjustments as necessary to maintain stability. The sliding surface is also robust to disturbances, uncertainties, and T3-FLS estimation errors, meaning that it is able to maintain stability even if there are variations in the system dynamics.

To better show the effectiveness of the suggested controller, the root-mean-square of tracking error (RMSE) is compared with some other related controllers, such as predictive controller [39], type-3 fuzzy controller (T3-FLC) [40], and SMC [7]. The results are shown in Table 2. We see that the RMSE of all errors x_{1e}, x_{2e}, and x_{3e} for the introduced controller is less than other closely related controllers. The suggested controller has the ability to observe the estimation errors and disturbances to eliminate their effect on accuracy. It should be noted that with newly developed programmable devices, the computational cost for various controllers is almost the same. As seen from Table 2, the execution times for different controllers are too close.
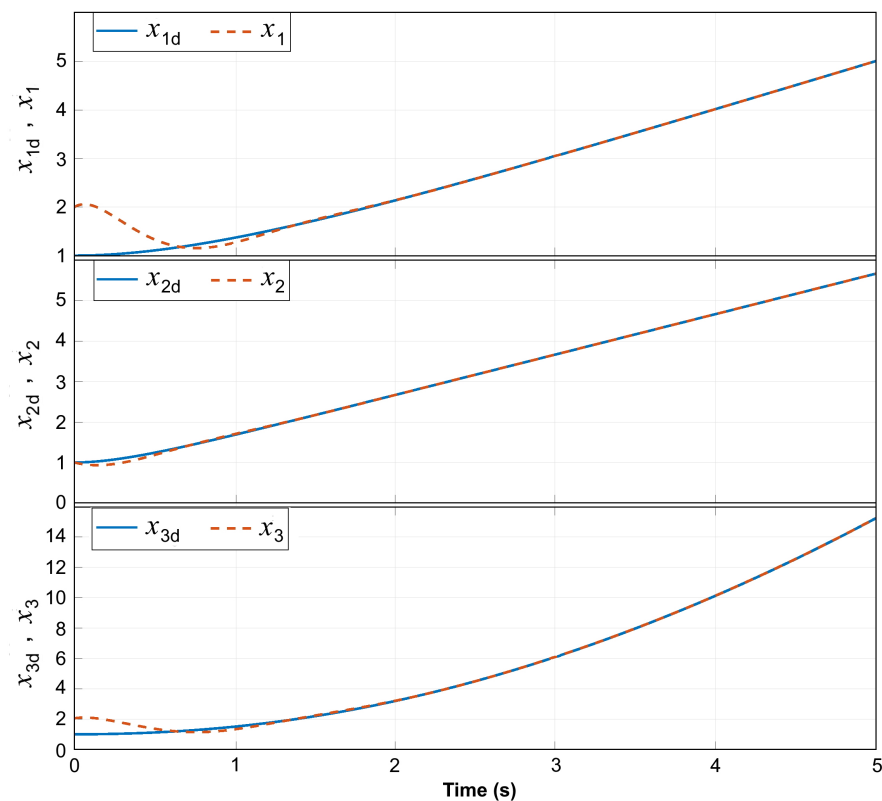

Figure 5. Trajectories of x_1 and x_{1d} (**top panel**), x_2 and x_{2d} (**middle panel**), and x_3 and x_{3d} (**bottom panel**).
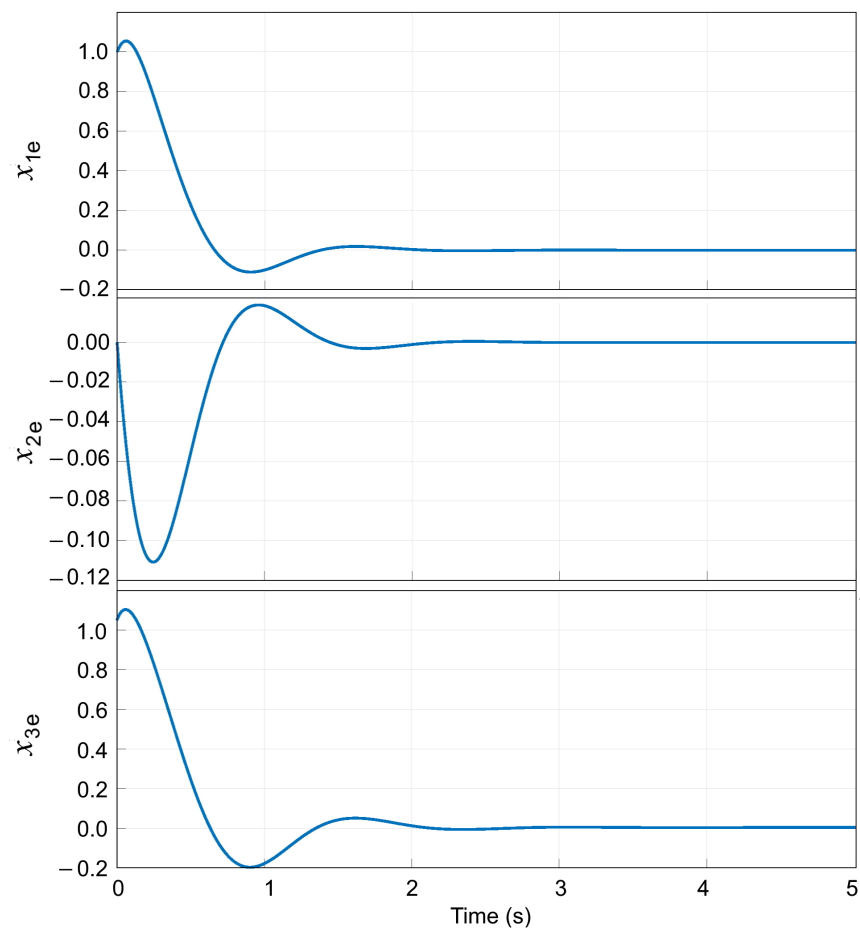
Figure 6. Tracking errors for x_1 (**top panel**), x_2 (**middle panel**), and x_3 (**bottom panel**).
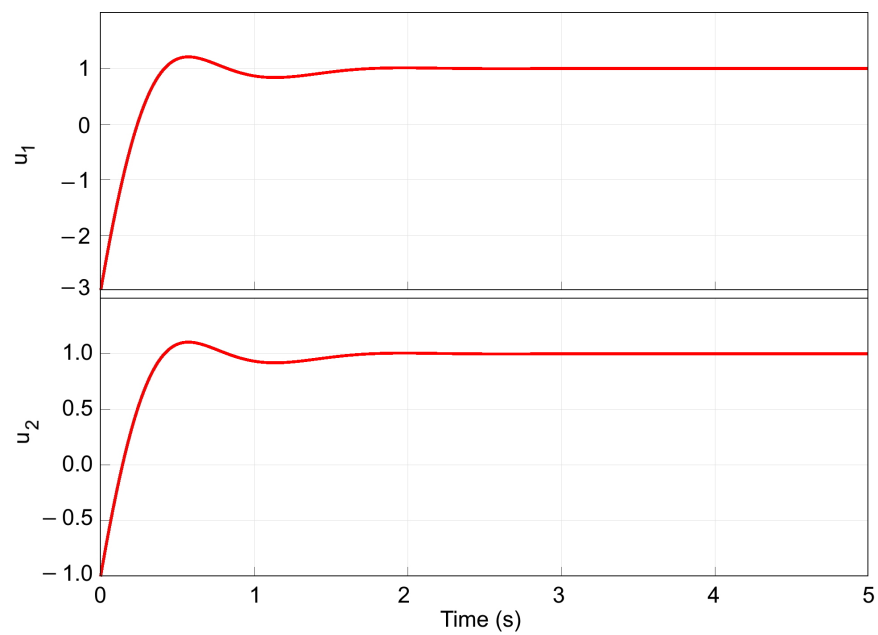
Figure 7. Controllers u_1 (**top panel**) and u_2 (**bottom panel**).
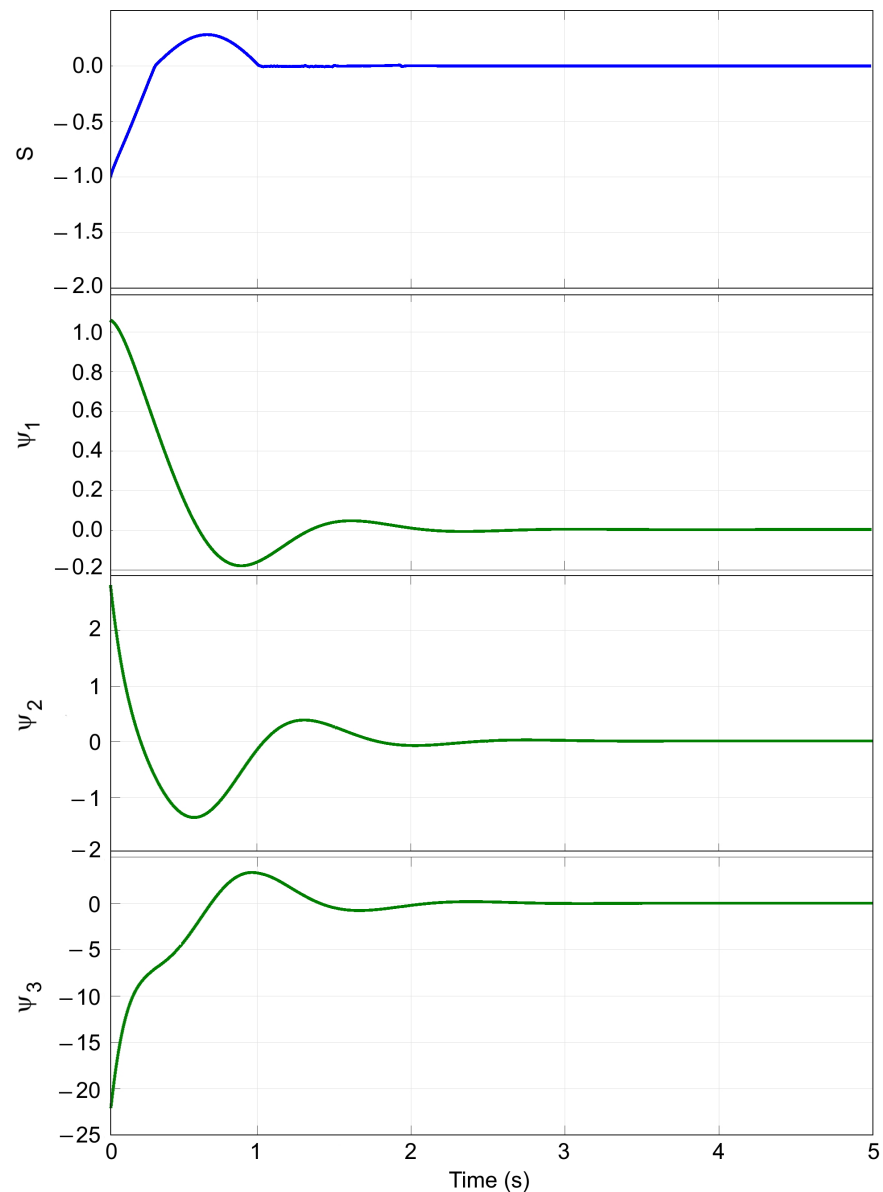
Figure 8. Sliding surfaces *s*, ψ_1, ψ_2, and ψ_3.

Table 2. Comparisons with other controllers.

	Tracking Errors			Execution Time (s)
	x_{1e}	x_{2e}	x_{3e}	
Predictive controller [39]	1.0154	0.2307	0.5674	0.1201
T3-FLC [40]	0.6974	0.1570	0.7954	0.1221
SMC [7]	0.8064	0.3145	0.7874	0.1101
Proposed controller	0.5014	0.0871	0.4871	0.1220

The suggested controller does not depend on the robot dynamics and parameters. The dynamics are estimated, and the estimation error is also considered in stability. There are a few free parameters in the controller that have a small effect on performance. These parameters are determined by trial and error. However, in future studies, the controller parameters can be optimized. To decrease the computational cost, the suggested approach can be combined with some new control systems such as event-triggered controllers [41], optimal controllers [42,43], new modeling [44], and fault-tolerant systems [45].

6. Conclusions

In this paper, the control of non-holonomic robots was studied. A new T3-FLS-based controller was presented. All of the dynamics of the robot were modeled by a proposed T3-FLS. Thus, the controller did not depend on the model of the robot. The estimation error of T3-FLS in modeling was considered in stability analysis. A new observer-based SMC was designed to eliminate the effect of modeling errors and other perturbations. The control was applied to the robot, and the results showed that the tracking system of NWR had good stability and was able to quickly adapt to changes in the environment. The control signals demonstrated rapid convergence, stability, and robustness to disturbances and uncertainties. The obtained trajectory of the sliding surfaces also showed a rapid convergence to the desired surface with minimal oscillations or overshoot and was robust to disturbances and uncertainties. One of the disadvantages of the controller is that the speed of tracking is not considered in the control scheme. Additionally, the rule forms of T3-FLS are constant and are not optimized. Therefore, for future studies, the advanced fast controllers can be developed using suggested ideas in this paper.

References

1. Chen, F.; Qiu, X.; Alattas, K.A.; Mohammadzadeh, A.; Ghaderpour, E. A New Fuzzy Robust Control for Linear Parameter-Varying Systems. *Mathematics* **2022**, *10*, 3319. [CrossRef]
2. Chu, X.; Ng, R.; Wang, H.; Au, K.W.S. Feedback Control for Collision-Free Nonholonomic Vehicle Navigation on SE (2) With Null Space Circumvention. *IEEE/ASME Trans. Mechatron.* **2022**, *27*, 5594–5604. [CrossRef]
3. Wang, Z.; He, D.; Zhang, Q.; Shi, J. Observer-based finite-time model reference adaptive state tracking control with actuator saturation. *Int. J. Control Autom. Syst.* **2020**, *18*, 2721–2733. [CrossRef]
4. Sarrafan, N.; Zarei, J. Bounded observer-based consensus algorithm for robust finite-time tracking control of multiple nonholonomic chained-form systems. *IEEE Trans. Autom. Control* **2021**, *66*, 4933–4938. [CrossRef]
5. Mathiyalagan, K.; Sangeetha, G. Finite-time stabilization of nonlinear time delay systems using LQR based sliding mode control. *J. Frankl. Inst.* **2019**, *356*, 3948–3964. [CrossRef]
6. Rojas-Cubides, H.; Cortés-Romero, J.; Coral-Enriquez, H.; Rojas-Cubides, H. Sliding mode control assisted by GPI observers for tracking tasks of a nonlinear multivariable Twin-Rotor aerodynamical system. *Control Eng. Pract.* **2019**, *88*, 1–15. [CrossRef]
7. Cen, H.; Singh, B.K. Nonholonomic wheeled mobile robot trajectory tracking control based on improved sliding mode variable structure. *Wirel. Commun. Mob. Comput.* **2021**, *2021*, 2974839. [CrossRef]
8. Pai, M.C. Disturbance observer-based global sliding mode control for uncertain time-delay nonlinear systems. *IETE J. Res.* **2022**, *68*, 3331–3340. [CrossRef]
9. Sun, Z.; Hu, S.; He, D.; Zhu, W.; Xie, H.; Zheng, J. Trajectory-tracking control of Mecanum-wheeled omnidirectional mobile robots using adaptive integral terminal sliding mode. *Comput. Electr. Eng.* **2021**, *96*, 107500. [CrossRef]
10. Naderolasli, A.; Shojaei, K.; Chatraei, A. Terminal sliding-mode disturbance observer-based finite-time adaptive-neural formation control of autonomous surface vessels under output constraints. *Robotica* **2023**, *41*, 236–258. [CrossRef]
11. Tourajizadeh, H.; Sedigh, A.; Boomeri, V.; Rezaei, M. Design of a new steerable in-pipe inspection robot and its robust control in presence of pipeline flow. *J. Mech. Eng. Sci.* **2020**, *14*, 6993–7016. [CrossRef]
12. Sanz, R.; García, P.; Díez, J.L.; Bondia, J. Artificial pancreas system with unannounced meals based on a disturbance observer and feedforward compensation. *IEEE Trans. Control Syst. Technol.* **2020**, *29*, 454–460. [CrossRef]
13. Zhai, J.Y.; Song, Z.B. Adaptive sliding mode trajectory tracking control for wheeled mobile robots. *Int. J. Control* **2019**, *92*, 2255–2262. [CrossRef]
14. Yu, J.; Zhao, Y. Global robust stabilization for nonholonomic systems with dynamic uncertainties. *J. Frankl. Inst.* **2020**, *357*, 1357–1377. [CrossRef]

15. Hamdy, M.; Abd-Elhaleem, S.; Fkirin, M. Adaptive fuzzy predictive controller for a class of networked nonlinear systems with time-varying delay. *IEEE Trans. Fuzzy Syst.* **2017**, *26*, 2135–2144. [CrossRef]

16. Vu, N.T.T.; Ong, L.X.; Trinh, N.H.; Pham, S.T.H. Robust adaptive controller for wheel mobile robot with disturbances and wheel slips. *Int. J. Electr. Comput. Eng. (IJECE)* **2021**, *11*, 336–346. [CrossRef]

17. Gharajeh, M.S.; Jond, H.B. Hybrid global positioning system-adaptive neuro-fuzzy inference system based autonomous mobile robot navigation. *Robot. Auton. Syst.* **2020**, *134*, 103669. [CrossRef]

18. Bi, M. Control of robot arm motion using trapezoid fuzzy two-degree-of-freedom PID algorithm. *Symmetry* **2020**, *12*, 665. [CrossRef]

19. Cuevas, F.; Castillo, O.; Cortés-Antonio, P. Generalized Type-2 Fuzzy Parameter Adaptation in the Marine Predator Algorithm for Fuzzy Controller Parameterization in Mobile Robots. *Symmetry* **2022**, *14*, 859. [CrossRef]

20. Mancilla, A.; García-Valdez, M.; Castillo, O.; Merelo-Guervós, J.J. Optimal fuzzy controller design for autonomous robot path tracking using population-based metaheuristics. *Symmetry* **2022**, *14*, 202. [CrossRef]

21. Chen, Y.; Zhao, T.; Dian, S.; Zeng, X.; Wang, H. Balance adjustment of power-line inspection robot using general type-2 fractional order fuzzy PID controller. *Symmetry* **2020**, *12*, 479. [CrossRef]

22. Chen, Y.H.; Chen, Y.Y. Nonlinear Adaptive Fuzzy Control Design for Wheeled Mobile Robots with Using the Skew Symmetrical Property. *Symmetry* **2023**, *15*, 221. [CrossRef]

23. Luviano-Cruz, D.; Garcia-Luna, F.; Pérez-Domínguez, L.; Gadi, S.K. Multi-agent reinforcement learning using linear fuzzy model applied to cooperative mobile robots. *Symmetry* **2018**, *10*, 461. [CrossRef]

24. Almasri, E.; Uyguroğlu, M.K. Modeling and trajectory planning optimization for the symmetrical multiwheeled omnidirectional mobile robot. *Symmetry* **2021**, *13*, 1033. [CrossRef]

25. Huang, H.; Xu, H.; Chen, F.; Zhang, C.; Mohammadzadeh, A. An Applied Type-3 Fuzzy Logic System: Practical Matlab Simulink and M-Files for Robotic, Control, and Modeling Applications. *Symmetry* **2023**, *15*, 475. [CrossRef]

26. Xu, S.; Zhang, C.; Mohammadzadeh, A. Type-3 fuzzy control of robotic manipulators. *Symmetry* **2023**, *15*, 483. [CrossRef]

27. Hua, G.; Wang, F.; Zhang, J.; Alattas, K.A.; Mohammadzadeh, A.; The Vu, M. A New Type-3 Fuzzy Predictive Approach for Mobile Robots. *Mathematics* **2022**, *10*, 3186. [CrossRef]

28. Peraza, C.; Ochoa, P.; Castillo, O.; Geem, Z.W. Interval-Type 3 Fuzzy Differential Evolution for Designing an Interval-Type 3 Fuzzy Controller of a Unicycle Mobile Robot. *Mathematics* **2022**, *10*, 3533. [CrossRef]

29. Wang, J.; Yang, M.; Liang, F.; Feng, K.; Zhang, K.; Wang, Q. An algorithm for painting large objects based on a nine-axis UR5 robotic manipulator. *Appl. Sci.* **2022**, *12*, 7219. [CrossRef]

30. Wang, B.; Shen, Y.; Li, N.; Zhang, Y.; Gao, Z. An adaptive sliding mode fault-tolerant control of a quadrotor unmanned aerial vehicle with actuator faults and model uncertainties. *Int. J. Robust Nonlinear Control* **2023**. [CrossRef]

31. Lu, C.; Gao, R.; Yin, L.; Zhang, B. Human-Robot Collaborative Scheduling in Energy-efficient Welding Shop. *IEEE Trans. Ind. Inform.* **2023**. [CrossRef]

32. Wang, J.; Liang, F.; Zhou, H.; Yang, M.; Wang, Q. Analysis of Position, pose and force decoupling characteristics of a 4-UPS/1-RPS parallel grinding robot. *Symmetry* **2022**, *14*, 825. [CrossRef]

33. Hou, X.; Zhang, L.; Su, Y.; Gao, G.; Liu, Y.; Na, Z.; Xu, Q.; Ding, T.; Xiao, L.; Li, L.; et al. A space crawling robotic bio-paw (SCRBP) enabled by triboelectric sensors for surface identification. *Nano Energy* **2023**, *105*, 108013. [CrossRef]

34. Gu, Q.; Tian, J.; Yang, B.; Liu, M.; Gu, B.; Yin, Z.; Yin, L.; Zheng, W. A novel architecture of a six degrees of freedom parallel platform. *Electronics* **2023**, *12*, 1774. [CrossRef]

35. Wang, B.; Zhu, D.; Han, L.; Gao, H.; Gao, Z.; Zhang, Y. Adaptive Fault-Tolerant Control of a Hybrid Canard Rotor/Wing UAV Under Transition Flight Subject to Actuator Faults and Model Uncertainties. *IEEE Trans. Aerosp. Electron. Syst.* **2023**. [CrossRef]

36. Wang, B.; Zhang, Y.; Zhang, W. A Composite Adaptive Fault-Tolerant Attitude Control for a Quadrotor UAV with Multiple Uncertainties. *J. Syst. Sci. Complex.* **2022**, *35*, 81–104. [CrossRef]

37. Hamdy, M.; Ibrahim, A.; Abozalam, B.; Helmy, S. Maximum Power Point Tracking for Solar Photovoltaic System Based on Interval Type-3 Fuzzy Logic: Practical Validation. *Electr. Power Compon. Syst.* **2023**, *51*, 1009–1026. [CrossRef]

38. Qasem, S.N.; Ahmadian, A.; Mohammadzadeh, A.; Rathinasamy, S.; Pahlevanzadeh, B. A type-3 logic fuzzy system: Optimized by a correntropy based Kalman filter with adaptive fuzzy kernel size. *Inf. Sci.* **2021**, *572*, 424–443. [CrossRef]

39. Wang, J.; Dong, H.; Chen, F.; Vu, M.T.; Shakibjoo, A.D.; Mohammadzadeh, A. Formation Control of Non-Holonomic Mobile Robots: Predictive Data-Driven Fuzzy Compensator. *Mathematics* **2023**, *11*, 1804. [CrossRef]

40. Alkabaa, A.S.; Taylan, O.; Balubaid, M.; Zhang, C.; Mohammadzadeh, A. A practical type-3 Fuzzy control for mobile robots: Predictive and Boltzmann-based learning. *Complex Intell. Syst.* **2023**, 1–14. [CrossRef]

41. Abd-Elhaleem, S.; Soliman, M.; Hamdy, M. Modified repetitive periodic event-triggered control with equivalent-input-disturbance for linear systems subject to unknown disturbance. *Int. J. Control* **2022**, *95*, 1825–1837. [CrossRef]

42. Yousef, H.A.; Hamdy, M.; Saleem, A.; Nashed, K.; Mesbah, M.; Shafiq, M. Enhanced adaptive control for a benchmark piezoelectric-actuated system via fuzzy approximation. *Int. J. Adapt. Control Signal Process.* **2019**, *33*, 1329–1343. [CrossRef]

43. Luo, R.; Peng, Z.; Hu, J. On model identification based optimal control and it's applications to multi-agent learning and control. *Mathematics* **2023**, *11*, 906. [CrossRef]

44. Karaduman, B.; Tezel, B.T.; Challenger, M. Rational software agents with the BDI reasoning model for Cyber–Physical Systems. *Eng. Appl. Artif. Intell.* **2023**, *123*, 106478. [CrossRef]
45. Xu, S.; Dai, H.; Feng, L.; Chen, H.; Chai, Y.; Zheng, W.X. Fault Estimation for Switched Interconnected Nonlinear Systems with External Disturbances via Variable Weighted Iterative Learning. *IEEE Trans. Circuits Syst. II Express Briefs* **2023**, *70*, 2011–2015. [CrossRef]